Tiny Integrated Network Analyzer for Noninvasive Measurements of Electrically Small Antennas

Buskgaard, Emil Feldborg; Krøyer, Ben; Tatomirescu, Alexandru; Franek, Ondrej; Pedersen, Gert F.

Aalborg Universitet

Tiny Integrated Network Analyzer for Non-Invasive Measurements of Electrically Small Antennas

Emil Buskgaard, Ben Krøyer, Alexandru Tatomirescu, Ondrej Franek, Gert Frølund Pedersen

Tiny Integrated Network Analyzer for Non-Invasive Measurements of Electrically Small Antennas

Emil Buskgaard, Ben Krøyer, Alexandru Tatomirescu, Ondrej Franek, Gert Frølund Pedersen

Abstract—Antenna mismatch and crosstalk are recurring issues in telecommunications. For electrically small antenna systems these are very hard to measure without affecting the radiation performance of the system and, consequently, the measurement itself. Electrically small antennas are found in many applications ranging from consumer electronics to industrial systems. We propose a radically new approach to characterize crosstalk and mismatch based on vector network analysis. By miniaturizing the network analyzer it can be integrated in the system under test eliminating the need for cables leaving the system. The tiny integrated network analyzer (TINA) is a stand-alone Arduino based measurement system utilizing the transmit signal of the system under test as its reference. It features a power meter with triggering ability, on-board memory, USB and easy extendibility with general purpose I/O. The accuracy and repeatability of the proposed system is documented through the repeatability of the calibration. To showcase the capabilities of the system, a measurement is done on a modified smart phone with the system inside. These early results show great promise for miniaturized network analysis. With the advances in software defined radio we can expect much more flexible and advanced integrated network analyzers in the coming years.

Index Terms—Measurement techniques, Electrically-small antennas, Vector network analysis, Antenna measurements, MIMO, Calibration

I. INTRODUCTION

THE advent of the Internet of things (IoT) brings a situation where a great number of various small devices are wirelessly connected in very diverse environments. Securing good radio performance for these networks is paramount as a unstable connection to a sensor could be problematic for i.e., the control of an industrial process or suboptimal performance of a battery powered device will decrease the battery life.

For many wireless systems the electrical size of the system is often much smaller than half the wavelength of the communication frequency. This means that their antennas are electrically small [1], [2]. Measurements on electrically small antennas (ESA) are challenging due to the high risk of interfering with the device under test (DUT) [3], [4]. Any metallic structure will couple to the antenna and change both the radiation pattern and the matching of the antenna. Furthermore these applications often have several antennas that are required to be decoupled and they often operate in highly dynamic environments where metallic objects or parts of a user's body enter the near field of the antennas.

All authors are with Section of Antennas, Propagation and Radio Networking (APNet), Department of Electronic Systems, Faculty of Engineering and Science, Aalborg University, DK-9220, Aalborg, Denmark ({eb, bk, ata, of, gfp}@es.aau.dk)

Accurate measurements of the coupling and reflection of electrically small antennas can help engineers to acquire vital information needed to create robust antenna systems. Such measurements can be used to verify that antenna systems can handle the mismatch that they will encounter during operation or to gauge the mismatch during operation for actively tuned antennas [5]–[8]. Current measurement techniques are not fit for electrically small antennas. The common approach is to measure the antenna impedance and coupling as S-parameters using a vector network analyzer (VNA). It relies on a VNA attached to the DUT by cables or optical fibers [9], [10]. When using coaxial cables, the cable will perturb the electrical fields close to the DUT [11]. By using an optical link this is prevented but also this approach has drawbacks. The authors are not aware of any commercial optical two-way link that is capable of measuring S-parameters and the implementations found are all encased in big metallic boxes.

Smaller VNA's exist on the market today. The miniVNA Tiny from mini Radio Solutions has a good frequency range of 1 MHz to 3 GHz. It is however still very big (66 x 66 x 28 mm) compared to the size of a phone or a tablet and it needs a USB connection to a PC to function. It is thus not truly wireless. [12] is another small USB connected VNA but it is even bigger and only reaches 1.3 GHz which is not enough for many modern wireless devices. All current VNA based options are thus not suitable for electrically small antenna systems at least if the frequency exceeds 1 GHz.

The proposed solution is to design a VNA that is small compared to the size of the DUT and can be integrated into the DUT. In this way the antenna S-parameters can be measured with minimal interference to the DUT. This new class of measurement equipment is dubbed the tiny integrated network analyzer, TINA. Obviously, a system that is reduced this much in size will not perform at the level of a full size VNA. It is believed that the most interesting insights to be gained from this new device are on the uncabled reflection of and coupling between ESA's, both in free space but particularly in proximity to users. For many applications, these figures are mostly interesting when their performance is bad meaning reflections higher than -6 dB or coupling higher than -10 dB. It is therefore not necessary to have a large dynamic range.

Although TINA as a class of measurement equipment serves a wide range of applications, a mobile phone is chosen to demonstrate the advantages of TINA. Performance of mobile phone antennas has been the subject of much discussion recently. Recent studies show that phone antennas in current smart phones are performing poorly both in free space and in the presence of the user [13].

The aim of the proof of concept is to measure the reflection of the main antenna and coupling between main and diversity antennas of the mobile phone (iPhone 5) during a live network call. During the call a test person will handle the phone in a natural fashion to replicate the user interaction occurring during a call or while browsing. It is important that the phone appears fully unchanged from the outside to enable the user to handle the phone naturally. To achieve this a smaller battery has been adapted to the phone to leave space in the phones battery compartment for the module to fit. It is thus fully embedded and no visible changes are made to the phone. For this proof of concept, the most important requirements are:

- The phone must be fully functional with original software and no noticeable change in performance.
- The phones appearance must be unchanged. This enables the most natural grip on the phone during the call giving the most realistic data possible.
- TINA must be able to sample both reflection and coupling of the antennas fast enough to analyze the changes in antenna performance induced by the user. 10 samples per second is believed to be fast enough.
- The system must be able to run for at least 30 minutes in a call. The battery must be large enough to power both the phone and TINA and the memory of TINA must be large enough to store the measurement data for 30 minutes of continuous measurements.

This article describes TINA and the first measurements made with it. In Section II the concept and implementation of the measurement setup are described, Section III shows the results of the calibration and the first measurement campaign conducted on the first phone with TINA embedded. Section IV discusses the accuracy of the calibration and the findings of the user study. Finally Section V concludes the study and presents the next steps.

II. METHODOLOGY

This section describes TINA as well as the other modifications that are made to the phone to enable the integration of TINA. Many modifications are necessary to achieve full integration of the module into the phone.

To minimize the size of TINA it has to be designed specifically for the application. TINA needs less dedicated circuitry if it can reuse the power supply, RF signal or digital processing of the DUT. In the case of a mobile phone a lot of options exist to use existing circuitry. The RF signal can be used as the reference of TINA if the phone is forced to operate in GSM mode. The GSM standard has a much lower power range (5 to 33 dBm in low band (LB) and 0 - 30 dBm in high band (HB)) than more recent standards lowering the requirement on dynamic range for TINA. Additional benefits of GSM is the time division duplexing (TDD) that can be used for timing of the measurements and constant envelope that due to the flat power level does not add to the dynamic range requirements for TINA.

GSM has a couple of negative features from the perspective of TINA. First of all GSM employs discontinuous transmission (DTX) meaning that the transmitter of the phone will not
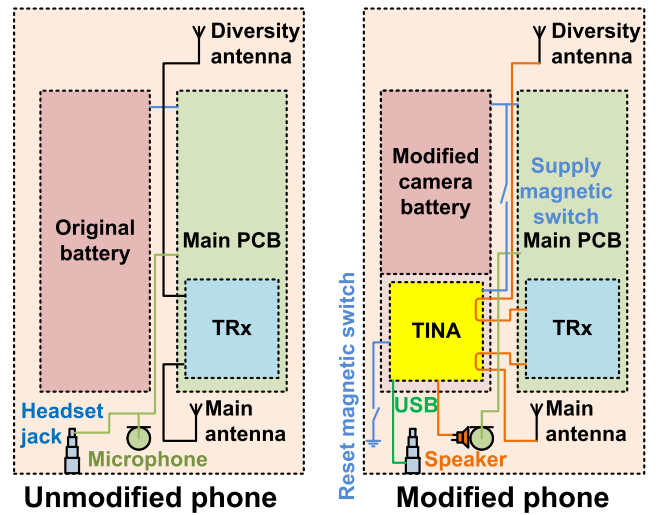

Fig. 1. Block diagram of the phone before and after the implementation of the module in the battery cavity of the phone.

transmit a burst if there is nothing to transmit. This is done to decrease the interference to other GSM users. To avoid bursts from being omitted, it is thus necessary to apply a signal to the microphone of the phone. As the microphone interface is digital, it is found to be very difficult to apply a signal directly into the microphone lines. Instead a small speaker from a hearing aid is inserted very close to the microphone of the phone and supplied with tones generated by TINA microprocessor. An additional problem is frequency hopping. No complete solution is found for this issue as TINA has no ability to gauge the frequency of the transmit (Tx) signal. The spread in Tx frequencies is thus seen as a source of uncertainty to the results.

To make room for TINA inside the phone the original battery is replaced by a smaller Casio NP-20 battery from a camera. This leaves $31 \times 34 \times 4$ mm^3 inside the phone that can house the module. Still the battery is capable of supplying both the phone and TINA for more than 1 hour of measurements.

The phone software does not allow us to use the phone's processors for logging the measured antenna parameters. Therefore TINA must include its own microprocessor system for data acquisition and interfacing.

The array of changes to the phone are shown in Fig. 1 where the standard phone is compared with the modified phone. Additional modifications include desoldering of the headset jack and using it for the USB link to the module, adding the hearing aid speaker very close to the main microphone and rerouting the antenna cables of the phone through TINA. Magnetic reed switches are used both for reset and on the battery supply of TINA. The reset switch closes in proximity of a magnet while the supply switch opens making it possible to power off TINA by placing the phone on a magnet. The addition of the power switch is necessary as TINA draws about 50 mA continuously resulting in severe battery drainage if left on overnight.
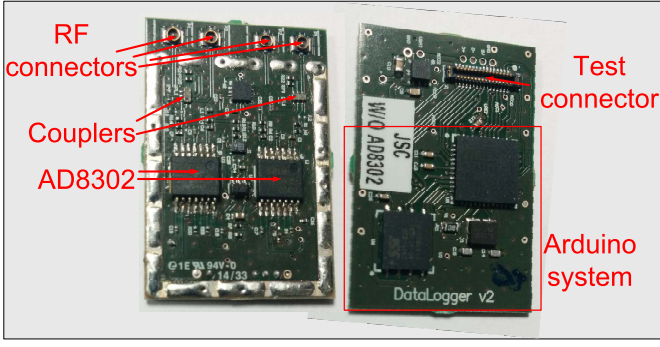
Fig. 2. Analog and digital side of TINA module. The analog side is normally covered by a shielding can which has been removed to reveal the RF circuitry.

Fig. 3. Block diagram of the analog part of TINA and its interconnects with the phone. All ports are linking to the digital part.

A. TINA

The measurement system, TINA, consists of a $20 \times 30 \times 3$ mm^3 module that is built into the phone as shown in Fig. 1. The size of TINA is chosen as a trade-off between the space needed in the phone and the ease of designing the module itself. TINA can be separated into two parts: a) An RF part doing the network analysis and b) a digital microprocessor system controlling the RF part, storing the data and handling the measurement timing and user interface. Both sides of the module are depicted in Fig. 2.

The RF part of TINA is shown in Fig. 3. It is connected to the antenna lines of the phone such that the antenna signals go through the bidirectional couplers and a part of the power is coupled to the module while the rest is delivered to the antennas. To limit the sensitivity of TINA outside the bands of interest, band pass filtering could be applied to the coupled signals. This would increase the robustness to WIFI, Bluetooth and other RF signals from the phone itself. It was however chosen to omit such filters as the space required for such filters was not found. Instead, the WIFI and Bluetooth signals are turned off on the phone leaving only the GSM signal active. Three RF signals are acquired from the couplers; The transmitted signal from the GSM radio, the reflected signal from the main antenna and the received signal on the diversity antenna.

The core of the RF signal processing is formed by two AD8302 gain and phase detectors. They can measure the amplitude and phase difference between two RF signals, INPA and INPB. This is a very old chip that suffers from several imperfections. In particular, the amplitude output of the AD8302 is dependent on both phase and amplitude difference between the two RF inputs as seen in TPC 24 of [14]. For this reason a full calibration across the whole Smith Chart and for several frequencies is chosen instead of any faster technique relying on predicted behavior of the system. The AD8302 has an input range of each of its RF inputs of -60 to 0 dBm. It can measure differences in input power of the two inputs up to ± 30 dB. This sets the upper bound of the dynamic range to 60 dB. The dynamic range is limited further by the 33 dB power range of the GSM signal resulting in a dynamic range that decreases from close to 60 dB at maximum power to less than 30 dB at the lowest power
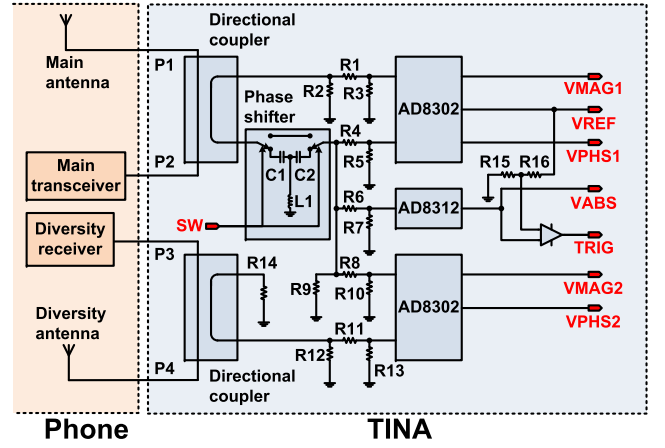
level of GSM. This is acceptable for the current application as reflections lower than -6 dB and coupling between the antennas lower than -10 dB are acceptable and both reflections and coupling lower than -20 dB are so far from the limit that they effectively are not of interest. The top AD8302 in Fig. 3 is comparing the forward and the reverse signal on the main antenna line. This gives us the reflection coefficient from the main antenna. The bottom AD8302 compares the signal from the main transceiver to the received signal on the diversity antenna. This gives the coupling between the two antennas. The outputs of the AD8302 are two voltage signals where one, VPHS, is proportional to the difference in phase between the two RF input signals and the other, VMAG, is proportional to the quotient of the amplitude of the two RF input signals.

$$\text{VPHS} = \|\angle\text{INPA} - \angle\text{INPB}\| , \quad \text{VMAG} = \frac{V_{\text{INPA}}}{V_{\text{INPB}}} \quad (1)$$

As Equation (1) shows, VPHS reports the absolute difference between INPA and INPB. Therefore $\angle\text{INPA} - \angle\text{INPB}$ will give the same voltage as $\angle\text{INPB} - \angle\text{INPA}$. This is not acceptable for this purpose and therefore a phase shifter in the form of a high pass filter is added to the signal from the transceiver. This will phase shift the signal by approximately 90° at 900 MHz and 45° at 1800 MHz. By switching the signal to either bypass the filter or go through it, two different phase results are obtained and the combination of these results is unique. The real phase can thus be determined by doing these two measurements.

All the RF signals from the couplers are attenuated through resistive networks to achieve the desired RF powers of between -60 and 0 dBm for all power control levels (PCLs) of the GSM system and all mismatches. The component values of all discrete components on Fig. 3 are listed in Table I. The couplers are delivered under NDA and can thus not be described in detail. They are 0.8 by 1.6 mm and characterized from 699 to 2690 MHz with an insertion loss smaller than 0.23 dB typical and 0.36 dB worst case. The coupling factor changes from -27 dB in low bands to -20 dB in high bands.

R1	0 Ω	R2	NM	R3	56 Ω	R4	130 Ω
R5	30 Ω	R6	130 Ω	R7	1 kΩ	R8	130 Ω
R9	3.3 kΩ	R10	30 Ω	R11	0 Ω	R12	NM
R13	56 Ω	R14	50 Ω	R15	1 kΩ	R16	13 kΩ
C1	3.9 pF	C2	3.9 pF	L1	9.1 nH		

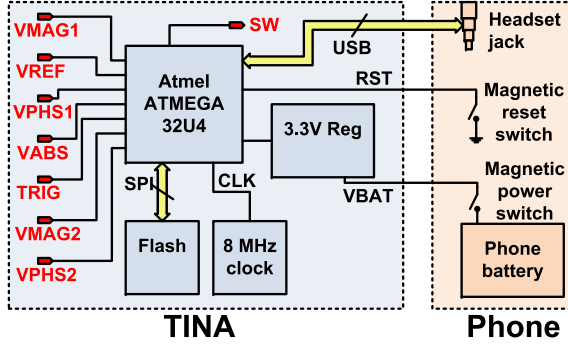Fig. 4. Block diagram of the digital part of TINA and its interconnects with the phone. All ports are linking to the digital part.
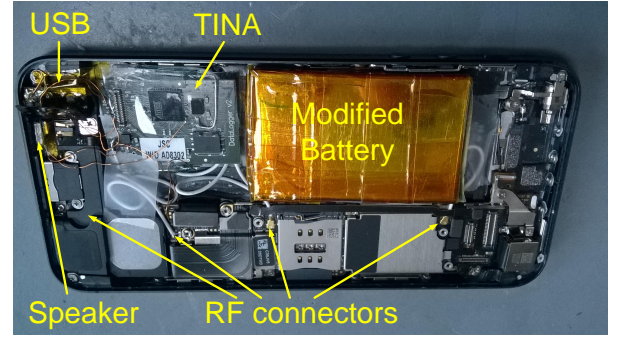

Fig. 5. Inside of the modified iPhone 5. Smaller battery, redirected antenna cables, USB connection through headset jack and a hearing aid speaker close to the microphone.

The resistive networks at the top and bottom are currently configured for minimum attenuation. R2 and R12 are not mounted, R1 and R11 are 0 Ω (short circuits) and R3 and R13 are, together with the input impedance of the AD8302's, presenting 50 Ω impedance to the traces. The resistive network on the branch from the phase shifter is used to split the power of the main transceiver signal into three branches; One for the top AD8302, one for the bottom AD8302 and one for an absolute power detector, the AD8312 [14] in the middle which is used to gauge the PCL of the phone on VABS and, together with a comparator, to generate a burst trigger signal, TRIG. The comparator gets a reference signal from the top AD8302 which is divided resistively to 200 mV, so when the output of the AD8312 exceeds 200 mV the trigger signal goes high. This corresponds to an output signal of about -5 dBm out of the main transceiver.

The five analog voltages from the three detectors are fed to the digital part of TINA along with the burst trigger and the reference voltage from the top AD8302. The digital part of TINA is depicted in Fig. 4. An Arduino [?] minimum system is implemented on TINA to control the measurements. By choosing the Arduino platform the programming is made substantially easier and many prebuilt functions can be used. The digital part controls the phase shifter in the RF part, reads the voltages with its ADC inputs and saves the data. The communication with TINA is handled via USB. To completely hide TINA inside the phone the USB connection is attached to the phones headset connector.

An interrupt routine is implemented to read the ADCs synchronized to the burst by using the TRIG signal from the RF part. This is the basis of the user test. When TINA is put into trigger mode it also generates a sequence of tones to the

hearing aid speaker to keep the GSM link active at all times. The level of the hearing aid speaker is adjusted such that it can be heard at the other end of a call but not by the user of the DUT.

On top of the Arduino minimum system the digital part contains an 8 MHz clock circuit, a voltage regulator to supply the module with 3.3 V and a memory chip for saving the data. The power for the module is obtained from the phones battery.

B. Test procedure

Based on the blocks described above, the measurement system is run and data about the phone are acquired. There are three main tasks to perform to retrieve the reflection and coupling parameters of the phone antennas: calibration, measurement and post processing. Their individual flow charts are depicted in Fig. 6 while a more detailed description is given in this section.

First task is to calibrate the module. TINA contains a large analog part that has certain tolerances. These tolerances affect the accuracy of the system and must therefore be calibrated. By calibrating the module in many impedance points across all phases, the inaccuracies of the components are taken into account. Both the AD8302's, the phase shifter, the resistive attenuator networks and the couplers add uncertainties, many of which are mismatch dependent. Therefore it is concluded that the full range of impedances must be calibrated. As the frequency of operation is also important, TINA is calibrated at both high, middle and low channel in both the EGSM and the DCS band. The calibration is done using the calibration setup shown in Figure 7. It consists of a computer running LabView, a signal generator, a circulator and an impedance tuner. Fig. 8 shows the two different setups that are made from these components; A) and C) for reflection (S11) calibration and B) and D) for coupling (S21) calibration. The list of equipment is included in Table II.

The tuner itself needs to be calibrated with the setup shown in Fig. 8 A). For this calibration, the standard Maury software is used to make an adaptive calibration. The number of calibration points is adaptively determined by the software and lies between 250 and 300 points depending on frequency. One issue with the tuner is that the maximum voltage standing wave ratio (VSWR) is lower than desired. With a maximum
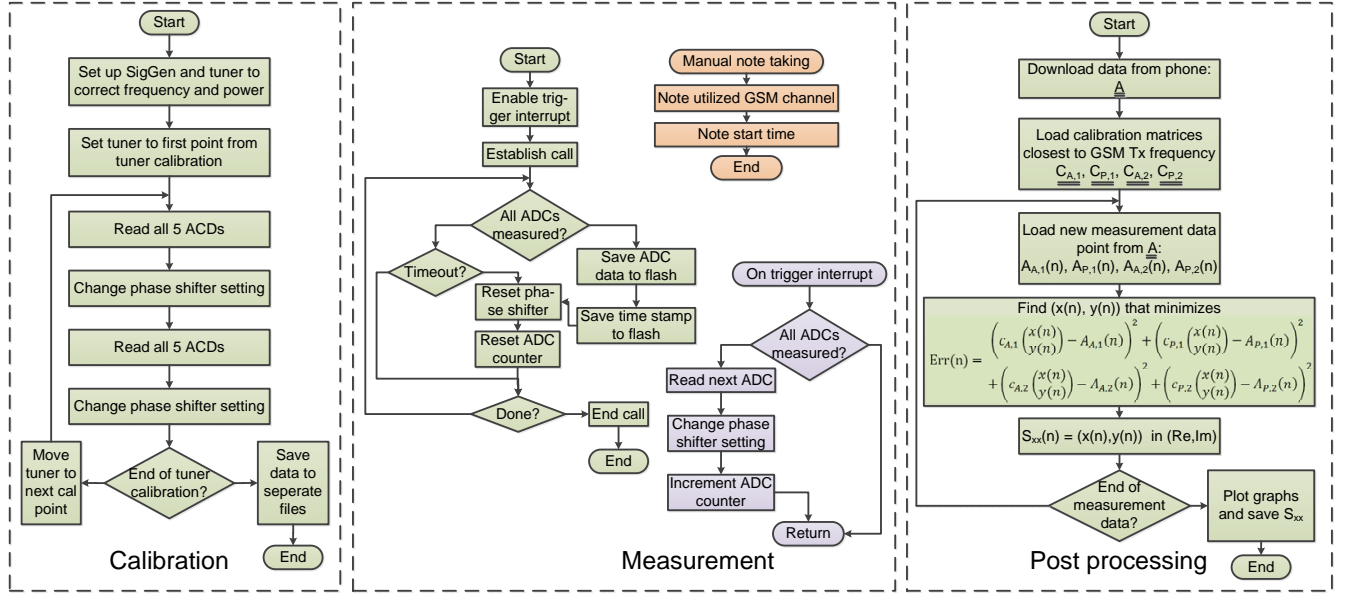
Fig. 6. Flow charts of the three main procedures in the system; The calibration of the module, the measurement inside the phone and the post processing of the results from the measurements.
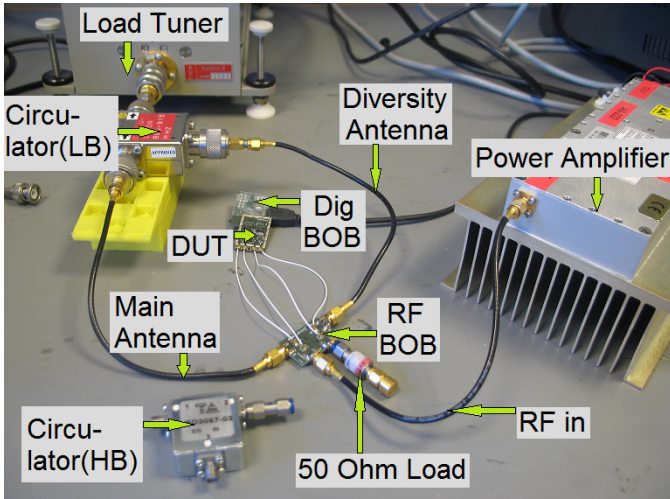

Fig. 7. Picture of the calibration setup. RF BOB and Dig BOB are break-out boards designed to make easy connections to TINA during calibration.
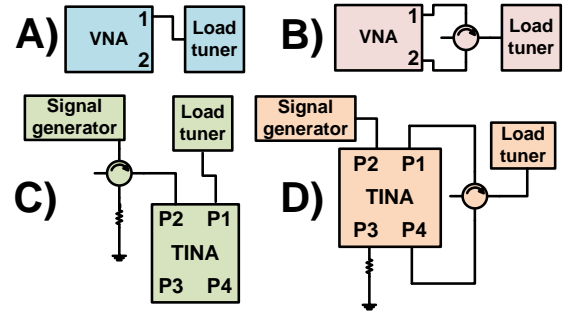

Fig. 8. Setup diagram for the module calibration. A) is for tuner calibration for the reflection branch and B) for the coupling branch of the module. C) and D) show the respective module calibration setups used for reflection and coupling.

TABLE II

EQUIPMENT USED FOR THE CALIBRATION OF THE MODULE

Instrument	Model
R&S Signal generator	SME 06 [15]
R&S Vector network analyzer	ZVB 8 [16]
Maury Impedance tuner	MT982B01 [17]
Circulator for 890 - 915 MHz	Celwave BC900
Circulator for 1805 - 1880 MHz	Temex BD3067-03

of 9:1 in EGSM and 7.5:1 in DCS the calibration can only cover return losses down to 1.9 dB in EGSM and 2.3 dB in DCS. It would have been desirable to be able to measure greater mismatches but this cannot be done with the current calibration method. Once the tuner is calibrated, the primary

branch of TINA is inserted as shown in Fig. 8 C) and the tuner is swept to exactly the same points as are used for the tuner calibration and the ADC's of TINA are read back. A calibration file is saved where the ADC values from TINA are linked to the reflection coefficient of the tuner. This file is later used for translation of the ADC points measured under test to S_{11}.

For the coupling branch of the module a slightly different calibration setup is required. Here the tuner is used to generate a reflected signal with a known phase and amplitude compared to the incoming signal. By feeding the signal into the tuner through the circulator, the reflected signal can be separated from the incoming signal and measured by Port 2 of the VNA as shown in Fig. 8 B). The tuner and circulator are then connected between the primary antenna port, P1, and the secondary antenna port, P4, of TINA as shown in Fig. 8 D). As for the reflection coefficient, the tuner is again swept through

all its' calibrated points and a file is saved that links the S_{21} measured in Fig. 8 B) to the ADC values of TINA for the corresponding tuner settings in Fig. 8 D).

The module only measures and stores ADC values. It is thus not needed to upload the calibration files to the module. Instead the calibration files are saved on a server for use during the post processing. A Matlab script is used to make an oversampled map of ADC values all across the Smith chart. A uniformly spaced matrix of 200 by 200 points is made by interpolating the measured ADC values.

To perform measurements the triggered mode is enabled through a serial command and thereafter the phone will record ADC values every time a burst is detected. The measurement time of TINA is very short. It is found to be possible to reliably measure three ADC values in each burst. It is thus chosen to measure both VMAG and VPHS from one AD8302 and VABS in the same burst. In the first burst VMAG1 and VPHS1 are measured with phase shifter setting 1 (SW1). In the next burst the same AD8302 is read with setting 2 of the phase shifter (SW2). In the two next bursts the same measurements are made for VMAG2 and VPHS2. The total measurement sweep of TINA takes 4 bursts or 18.46 ms. A sample rate of more than 50 Hz is therefore possible. 10 Hz is deemed enough to catch even fast changes and to limit the memory usage this is the chosen sampling rate.

The timing of the bursts is recorded by adding a time stamp for each complete ADC sweep. The time stamps run off an internal clock and are thus not very precise but only an approximate timing information is needed. The only use of the time stamps is finding the approximate time of an event to find the cause of the event on video recordings of the measurement. To convert the internal clock to that of the computer a time stamp is recorded when the triggered mode is enabled and for each full sweep of ADC values. By comparing the time between these time stamps to the difference in value, the time step of the module clock can be found.

After a user measurement is done the data are downloaded to the computer and the post processing tools are used to convert the raw ADC values from the measurement to reflection and transmission coefficients. The post processing tool uses the calibration files to do the conversion according to the formula shown in the biggest green box of Fig. 6. The function determines, for every time step in the measured data, the squared difference between the measured ADC value and each point in the corresponding calibration matrix. It then adds these difference matrices for each phase shifter setting and both amplitude and phase measurements to get an overall difference matrix. By finding the minimum of this matrix, the least square residual is found and this point is believed to be the closest to point in the matrix to the measured ADC values. Since the matrix is a 200 by 200 value matrix uniformly spaced across the Smith Chart, the index of the least square residual can be converted to a complex S-parameter value simply by counting the distance in indices from the center of the Smith Chart and divide it by 100. The calibration files map the ADC values of the different ADC's across the Smith chart. Ideally VMAG should be constant for constant VSWR and VPHS should change linearly with phase. As earlier mentioned, this
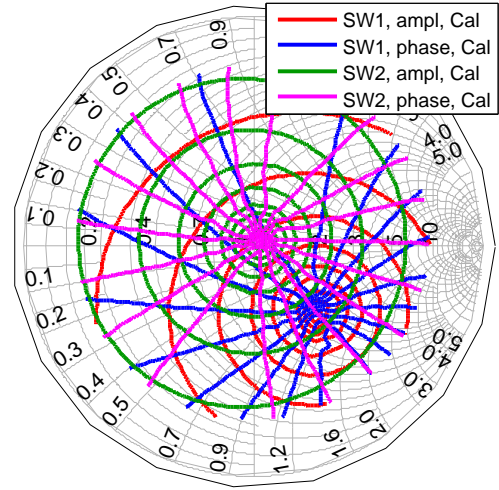

Fig. 9. Contour plot of the calibration data in the impedance Smith Chart with $Z_L = 50\Omega$. SW1 is with phase shifter in setting 1 and SW2 is with phase shifter in setting 2.

is not the case for the AD8302 as can be seen on Fig. 9. Clearly the calibration done with switch setting 2 gives the most optimum performance where the maximum value is close to the center of the Smith chart. The offset with switch setting 1 is larger because the high pass filter of the phase shifter is close to its cutoff frequency. This results in an impedance far from 50 Ω, which impairs the performance of TINA all together. For a future design, a delay line could be used for phase shifting to avoid this effect.

Fig. 10 shows an example of the output of the post processing algorithm. An ADC sweep is chosen from the output file of the phone. The values were $VPHS_{SW1} = 232$, $VMAG_{SW1} = 518$, $VPHS_{SW2} = 343$ and $VMAG_{SW2} = 514$. The calibration contours equal to these values are highlighted in Fig. 10. As can be seen the $VMAG_{SW2}$ contour crosses the $VPHS_{SW2}$ contour in two places. The $VPHS_{SW1}$ contour coincides with the two other only in the upper crossing point. This is a clear indicator that this is the point of interest. The shown example is for the reflection coefficient but exactly the same procedure is used for the coupling coefficient.

When all ADC sweeps in the measurement series have been converted to reflection and coupling coefficients, a full series of coefficients versus time is obtained. This can be analyzed to find the range and rate of change of the coefficients. The following part contains the full set of data and analyses that were obtained from the initial measurement campaign.

III. RESULTS

This section contains the results that are obtained from the test setup described in the previous section. The results are split into two parts: a calibration accuracy study and a set of preliminary user data collected using TINA inside the iPhone.

A. Calibration accuracy

It is chosen to calibrate at low, mid and high channel for the GSM900 and the GSM1800 bands as these are the bands that are in use for the 2G networks in Denmark. The module
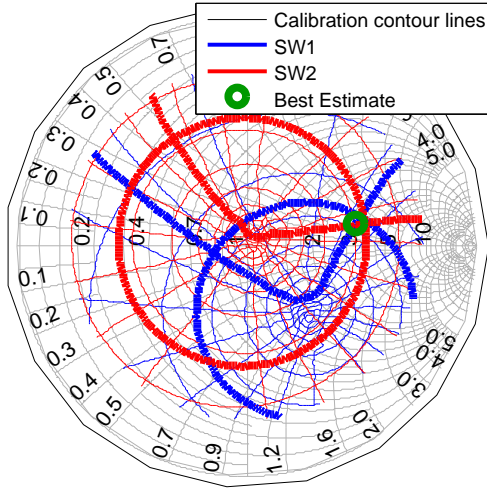
Fig. 10. Estimation of the reflection coefficient based on calibration data and a set of measured data points from the phone plotted in an impedance Smith Chart normalized to 50 Ω. The highlighted contours are the calibration contours matching the measured data points.

Fig. 11. The difference in amplitude calibration between 0 dBm and 30 dBm S_{11} calibration power for DCS band on TINA1 plotted in an impedance Smith Chart with $Z_L = 50\Omega$. The 0.5, 1 and 2 dB contour lines are shown as well as the constant VSWR circles for 2:1 and 3:1. The error is less than 0.5 dB for the majority of the calibration points with a very sharp spike in error close to the center of the Smith Chart. The black markers are showing the actual calibration points.

is designed to support all power levels of the 2G standard (5 to 33 dBm in GSM900 and 0 to 30 dBm in GSM1800). To ensure accurate results, the first modules, TINA1 and TINA2, are calibrated at 0, 10, 20 and 30 dBm for high band and 5, 14, 24 and 33 dBm for low band.

To verify that the calibration is repeatable and to investigate the reference power dependence of the calibration, a comparison is made between the calibration values for the highest and the lowest reference power level. Figures 11 and 12 show an example of a comparison. Here, TINA calibration at 1747 MHz and for switch setting 2 is chosen. The contour lines for selected differences are plotted along with the constant VSWR circles for 3:1 and 2:1. These two VSWR circles are plotted because they represent the -6 dB and -10 dB reflection/coupling level which are the most important levels when testing the phone. Finally, to illustrate the quantity and position of the calibration points, the complete calibration point constellation is plotted on top as black markers. It can be seen on these figures that the main uncertainty is concentrated where the reflected/coupled power is low. For the power, this is well inside the smallest VSWR circle meaning that the S-parameters are far below -10 dB. The uncertainty on phase is more spread out when looking at the range from 1 to 4 degrees.

The cumulative distribution function (CDF) of the difference in calibration values between highest and lowest power level can be seen in Figures 13 and 14 for amplitude and phase calibration, respectively. Only the minimum and maximum powers (0 and 30 dBm for DCS and 5 and 33 dBm for EGSM) are used since this gives the worst case error which is especially centered around the middle of the Smith Chart where the reflected and coupled signals get below the sensitivity of the AD8302. Here the calibration difference between the maximum and minimum power level can reach the full power difference between lowest and highest power, when the reflection or coupling reaches the noise floor. Any power
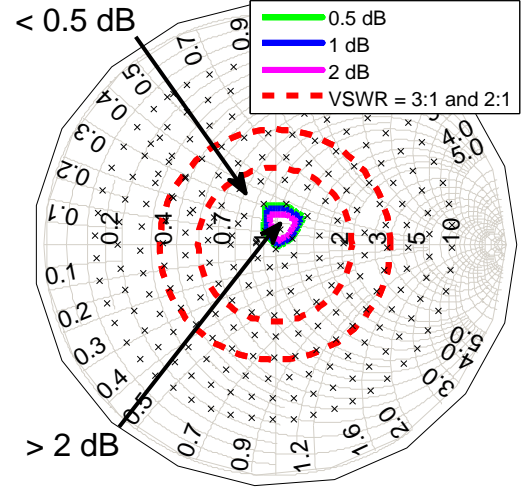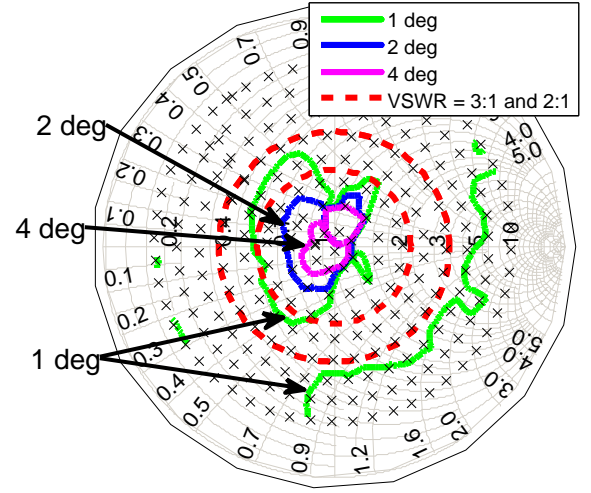

Fig. 12. The difference in phase calibration between 0 dBm and 30 dBm S_{11} calibration power for DCS band on TINA1 plotted in an impedance Smith Chart with $Z_L = 50\Omega$. The 1, 2 and 4 degrees contour lines are shown as well as the constant VSWR circles for 2:1 and 3:1. The black markers are showing the actual calibration points.

level in between will give less error. Each CDF is made based on all calibration points at all frequencies of the band with both switch settings and for both S_{11} and S_{21}. These plots do thus, collectively on all four non-temperature dependent graphs, incorporate the complete comparison between highest and lowest power level for all conditions on both modules.

TINA2 has also been calibrated in high band (HB) at 10°C and 55°C as well. The CDF of the variation over temperature can be seen in Figures 13 and 14 too.

B. User test results

As an overall system test a short measurement series is made with the modified phone for a small series of use
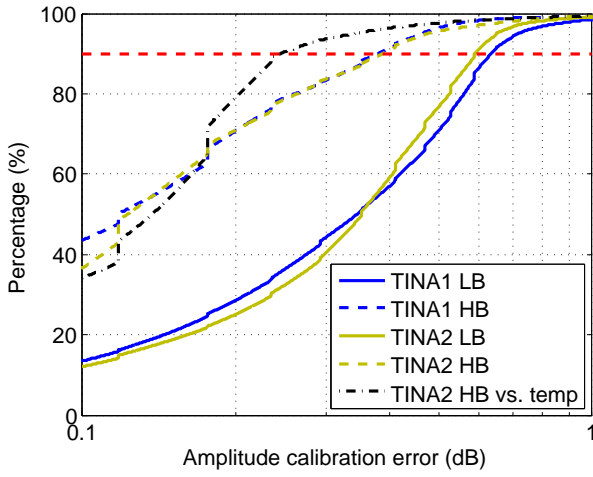
Fig. 13. Cumulative density function (CDF) of the variation for amplitude calibration for high and low band on two different modules. The black curve is showing variation over temperature between 10°C and 55°C.
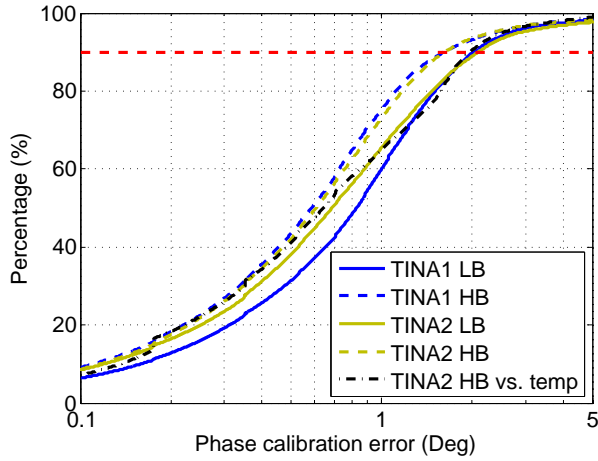

Fig. 14. Cumulative density function (CDF) of the variation for phase calibration for high and low band on two different modules. The black curve is showing variation over temperature between 10°C and 55°C.

cases. A time series of the magnitude of the reflection and coupling is plotted in Fig. 15. Fig. 16 shows the phase of the reflection and coupling between the phone's antennas for the same measurement. The measurement consists of a period where the phone is left on a Styrofoam block to measure the S-parameters in free space. Afterwards the phone is placed on a copper plate to measure it in a harsh but static environment. Finally the phone is handled by a test person who tries to change grips as much as possible to achieve a very dynamic user scenario.

IV. DISCUSSION

From the calibration data obtained for this study it is seen that the calibration accuracy is quite good. The calibration values change mostly close to the center of the Smith Chart. The region with significant changes is well within the 2:1 constant VSWR circle and thus only when the match is very good will these inaccuracies be seen. A difference of a dB
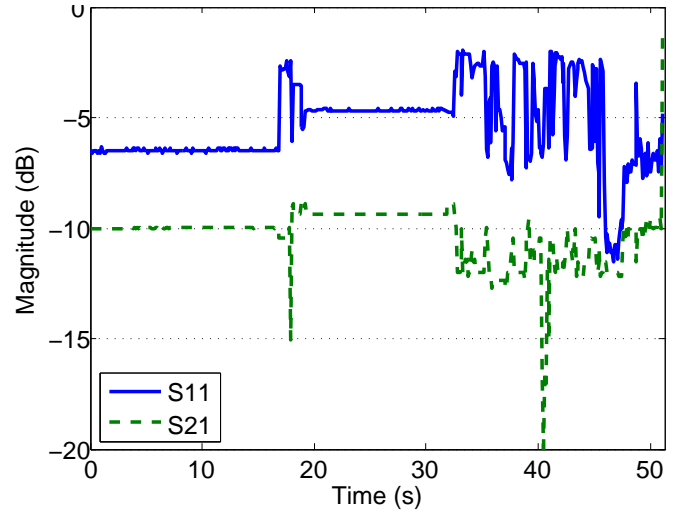

Fig. 15. Magnitude of the mismatch of the main antenna and coupling between the antennas versus time measured on the iPhone5 with TINA during test with a user.
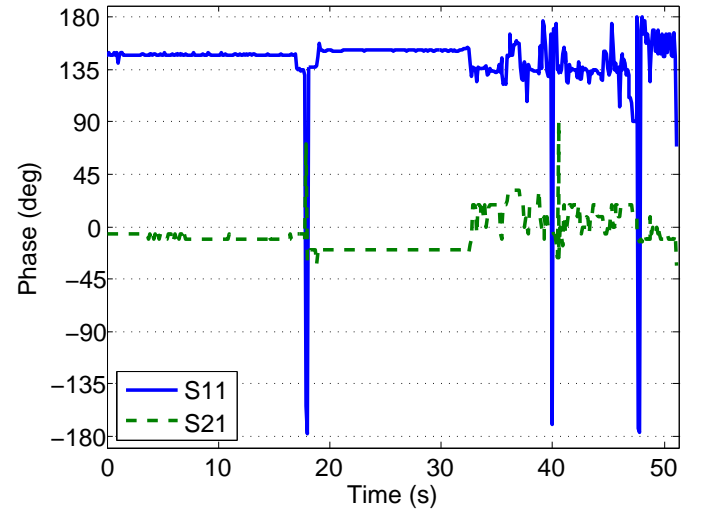

Fig. 16. Phase of the mismatch of the main antenna and coupling between the antennas versus time measured on the iPhone5 with TINA during test with a user.

does not matter in this region where the reflection is already down to -20 dB. As for the phase difference, it is more spread out in the Smith Chart. Since the main focus of this study is on accurately determining the magnitude of the reflection and coupling it is chosen to accept the error in phase.

90% of the values are within 0.6 dB for the amplitude and 2° for the phase. This is the worst case error due to difference in transmit power if the same calibration data are used for all power levels. It can be minimized by reading the on-board power meter for each burst and applying the calibration values obtained at the closest PCL. However, an error of this magnitude is considered acceptable and shows that the attenuation of the signals in the RF part of TINA is well adjusted to the power range in GSM. As can be seen in Figures 13 and 14 there is a comparable difference across temperatures from 10°C to 55°C. This is accepted as an added

uncertainty and thus the temperature inside the phone is not measured.

The highest inaccuracies are recorded close to the center of the Smith chart where the reflection and coupling are low. In this area of the Smith chart very small absolute changes lead to large changes in dB. It is thus expected that the inaccuracy in dB is high for this region.

As can be seen from Figures 15 and 16, the effect of the surrounding environment is clearly seen on the measured S-parameters. When the phone is left on the Styrofoam block, the magnitudes of the mismatch and coupling are very stable at -6.5 dB and -10 dB, respectively. These levels are in line with the normal design goal of mobile phone antennas of lower than -6 dB reflection. The phase of the S-parameters is quite stable which is to be expected since the phone is in a very stable position with no physical interaction. The influence of frequency hopping is not seen. This is because the frequency spread of the hopping sequence is only a few MHz which translate into negligible phase shifts for the RF line length of TINA.

When the phone is moved onto the copper plate, the mismatch changes to -4.7 dB. The coupling changes to -9.3 dB. It is to be expected that the reflection will be more dominant on the highly conductive surface. Still the coupling between the antennas is slightly increased and taking into account the reflection this means that a much larger portion of the emitted signal of the main antenna is absorbed by the diversity antenna. For this scenarios the phase is very stable as well.

For the final scenario, where the user is handling the phone and changing the grip rapidly, it is seen that the S-parameters of the antennas are also very fluctuating. The performance is generally poor with reflections often reaching -3 dB and worse. This is in line with previous studies on the iPhone5 that show extensive performance degradation in the presence of the user [18]. At the end of the measurement, a section with low reflection is recorded. In this section, the lossy tissue of the user is believed to absorb so much power that the match of the antenna is improved.

V. CONCLUSION

This study shows an original approach to S-parameter measurements on electrically small antennas. A system has been designed and implemented that can measure reflection and coupling for a two-antenna system. It is proposed for any small wireless system such as wireless sensors, mobile phones and wireless Internet devices.

To demonstrate the principle of the system, it is built into a fully functional commercially available phone. The system can measure the S-parameters of the phone antennas while the phone is in a call. The system consists of a main board, TINA, containing RF circuitry to measure amplitude and phase of both the reflection on the main antenna and the coupling to the diversity antenna. This is very hard to measure with a normal VNA because of the cable effect and even more challenging on a production phone with a user interacting with the phone.

The initial calibration data collected for TINA show good stability over temperature and phone output power. With an accuracy of approximately 0.6 dB and $2°$ for 90% of the measurement points, TINA can easily estimate any mismatch and coupling coefficient accurately enough for designing an active antenna tuner.

Even though the measurement system must be designed specifically for the DUT it is still seen as the best way to achieve accurate user test results. Any other method known to the authors either include cables or optical fibers obstructing the user. If one could fit a fully coherent transceiver inside the DUT it should in principle be possible to extract the phase and amplitude of the reflection by adding a coupler and using the receiver to demodulate the reflected wave from the antenna. Such capabilities could exist in the GSM transceiver of some modern smart phones but they are not available to the research community.

The introduction of this new measurement system enables tests that would otherwise be impossible to make. It will be possible to investigate the dynamics of the user effect without having obstructing cables hanging out of the phone. This enables true blind testing of the phones eliminating the risk that users may handle the phone differently because they know that the antennas are being tested.

REFERENCES

[1] H. Wheeler, "Small antennas," *IEEE Transactions on Antennas and Propagation*, vol. 23, no. 4, pp. 462–469, Jul 1975.

[2] M. Salehi and M. Manteghi, "Transient characteristics of small antennas," *IEEE Transactions on Antennas and Propagation*, vol. 62, no. 5, pp. 2418–2429, May 2014.

[3] W. Kotterman, G. Pedersen, K. Olesen, and P. Eggers, "Cable-less measurement set-up for wireless handheld terminals," in *12th IEEE International Symposium on Personal, Indoor and Mobile Radio Communications*, vol. 1, Sep 2001, pp. B–112–B–116 vol.1.

[4] T. H. Loh, M. Alexander, P. Miller, and A. Lopez Betancort, "Interference minimisation of antenna-to-range interface for pattern testing of electrically small antennas," in *Proceedings of the Fourth European Conference on Antennas and Propagation (EuCAP)*, April 2010, pp. 1–5.

[5] D. Ji, J. Jeon, and J. Kim, "A novel load mismatch detection and correction technique for 3g/4g load insensitive power amplifier application," *IEEE Transactions on Microwave Theory and Techniques*, vol. 63, no. 5, pp. 1530–1543, May 2015.

[6] S. Sussman-Fort and R. Rudish, "Non-foster impedance matching of electrically-small antennas," *IEEE Transactions on Antennas and Propagation*, vol. 57, no. 8, pp. 2230–2241, Aug 2009.

[7] P. Sjoblom and H. Sjoland, "Constant mismatch loss boundary circles and their application to optimum state distribution in adaptive matching networks," *IEEE Transactions on Circuits and Systems II: Express Briefs*, vol. 61, no. 12, pp. 922–926, Dec 2014.

[8] A. van Bezooijen, M. de Jongh, C. Chanlo, L. Ruijs, F. van Straten, R. Mahmoudi, and A. van Roermund, "A gsm/edge/wcdma adaptive series-lc matching network using rf-mems switches," *IEEE Journal of Solid-State Circuits*, vol. 43, no. 10, pp. 2259–2268, Oct 2008.

[9] R. Lao, W. Liang, Y.-S. Chen, and J. Tarng, "The use of electro-optical link to reduce the influence of RF cables in antenna measurement," in *IEEE International Symposium on Microwave, Antenna, Propagation and EMC Technologies for Wireless Communications*, vol. 1, Aug 2005, pp. 427–430 Vol. 1.

[10] B. Yanakiev, J. Nielsen, M. Christensen, and G. Pedersen, "Long-range channel measurements on small terminal antennas using optics," *IEEE Transactions on Instrumentation and Measurement*, vol. 61, no. 10, pp. 2749–2758, Oct 2012.

[11] S. Saario, D. Thiel, J. Lu, and S. O'Keefe, "An assessment of cable radiation effects on mobile communications antenna measurements," in *IEEE Antennas and Propagation Society International Symposium*, vol. 1, July 1997, pp. 550–553 vol.1.

[12] Gerfried Palme, *Measurements with the DG8SAQ VNWA 2/3 Vector Network Analyzer*, October 2015.

[13] A. Tatomirescu and G. Pedersen, "Body-loss for popular thin smart phones," in *7th European Conference on Antennas and Propagation (EuCAP)*, April 2013, pp. 3754–3757.

[14] *AD8302, LF2.7 GHz RF/IF Gain and Phase Detector*, Analog Devices, Inc., 2002, Data Sheet: Rev. A.

[15] *Rohde and Schwarz SME06 Operating Manual*, Rohde and Schwarz GmbH, 1999, Data Sheet: 1039.1856.12-14-.

[16] *Rohde and Schwarz ZVB Network Analyzer*, Rohde and Schwarz GmbH, 2011, Data Sheet: v08.02.

[17] *MT982 SERIES SENSOR TUNERS*, Maury Microwave Inc, 2012, Data Sheet: 4T-078.

[18] A. Tatomirescu and G. Pedersen, "User body loss study for popular smartphones," in *9th European Conference on Antennas and Propagation (EuCAP)*, 2015.